PET/CT: Challenge for Nuclear Cardiology*

Markus Schwaiger, MD; Sibylle Ziegler, PhD; and Stephan G. Nekolla, PhD

Nuklearmedizinische Klinik und Poliklinik, Klinikum rechts der Isar der TU München, Munich, Germany

This review focuses on the clinical potential of PET/CT for the characterization of coronary artery disease. We describe the technical challenges of combining instrumentations with very different imaging performances and speculate on future clinical applications in the field of cardiology.

Key Words: basic cardiology; technical cardiology; clinical cardiology; PET/CT; cardiac; imaging

J Nucl Med 2005; 46:1664–1678

Cardiovascular imaging has witnessed rapid growth in recent years. Several techniques compete for the diagnostic and prognostic workup of patients with proven or suspected coronary artery disease (CAD). Among these, myocardial perfusion imaging (MPI) has become the invasive diagnostic test most often applied in the United States. This success is based on the functional characterization of CAD. Gould et al. first described the importance of coronary flow reserve measurements in the clinical evaluation of CAD in the 1970s when they demonstrated that measuring coronary artery stenosis diameters does not predict the functional severity of CAD (*1*). Adding functional parameters such as blood flow reserve allows the stratification of coronary artery stenosis in hemodynamically significant or nonsignificant lesions. With the introduction of tomographic imaging approaches such as SPECT, it became possible to assess quantitatively the extent and severity of perfusion abnormalities (*2*). The success of MPI has been further enhanced by demonstrating not only the diagnostic but also the prognostic value of functional parameters. The low likelihood of cardiovascular events in patients with normal stress perfusion scintigraphy and the incremental value of exercise-induced perfusion abnormalities in comparison with electrocardiography-treadmill stress testing helped to convince the cardiology community to apply this test as a "gatekeeper" for invasive procedures (*3–5*). However, despite this clinical success, significant limitations of SPECT perfusion imaging remain. First, the radiotracers currently used for perfusion imaging do not exhibit ideal physiologic characteristics. The extraction fraction of ^{99m}Tc-labeled flow markers by the myocardium is relatively low and further decreases at higher flow rates (*6*). Second, the lack of accurate attenuation correction (AC) leads to artifacts reducing the specificity of SPECT in defining regional perfusion abnormalities (*7,8*). Correction methods using external transmission sources have been developed, but their use still has to be considered experimental (*9*).

In parallel with SPECT, PET has been developed as a clinical imaging tool for the quantitative assessment of myocardial perfusion and for the characterization of tissue viability in patients with advanced CAD. However, because of its high cost and lack of reimbursement in many countries, PET has never reached the same level of clinical acceptance as SPECT. Because PET is currently experiencing rapid growth as an imaging modality in oncology, the availability of PET instrumentation in many imaging departments is opening new opportunities for its application to cardiology. For both cardiac and oncologic applications, AC is an integral part of PET procedures. The use of external radiation sources for transmission measurements significantly prolongs the acquisition time for cardiac or oncologic examinations. However, to shorten the time of attenuation measurement, the idea of combining PET instrumentation with a CT scanner emerged. Townsend and Cherry first realized the combination of both imaging modalities in 2001 (*10*). This development was paralleled by the dramatic improvement of CT technology yielding multislice helical data acquisition to support whole-body PET (*11,12*). PET/CT has rapidly gained acceptance in the oncology community not only by providing efficient measurements of attenuation but also by allowing the integration of morphologic and metabolic information for detection, staging, and therapy control (*13*). The intention of using CT exclusively for AC is being increasingly replaced by the concept of applying both PET and CT at their fullest diagnostic potential. Adding the diagnostic range of cardiovascular CT to PET has opened a new dimension for cardiac imaging. Combining coronary calcification, noninvasive coronary angiography, and structural definition of cardiac and vascular

Received Aug. 4, 2005; revision accepted Aug. 22, 2005.

For correspondence or reprints contact: Markus Schwaiger, MD, Nuklearmedizinische Klinik und Poliklinik, Klinikum rechts der Isar der TU München, Ismaninger Strasse 22, 81675 München, Germany.

E-mail: M.Schwaiger@lrz.tu-muenchen.de

*NOTE: FOR CE CREDIT, YOU CAN ACCESS THIS ACTIVITY THROUGH THE SNM WEB SITE (http://www.snm.org/ce_online) THROUGH OCTOBER 2006.

TABLE 1
Characteristics of Scintillation Crystals for PET

Characteristic	BGO ($Bi_4Ge_3O_{12}$)	LSO (Lu_2SiO_5:Ce)	GSO ($GdSiO_5$:Ce)
Density (g/cm^3)	7.1	7.4	6.7
Effective Z	75	65	59
Attenuation length at 511 keV (mm)	10.4	11.4	14.1
Light yield (photons/MeV)	9,000	26,000	10,000
Decay time (ns)	300	40	60
Emission (nm)	480	420	440

tissues with PET data will contribute to a new comprehensive imaging procedure in cardiology.

PET IMAGING

PET technology excels because of its high sensitivity, homogeneous spatial resolution, and potential for quantitation of tissue tracer concentration. PET technologies have advanced with regard to detector material, data acquisition mode, and data processing. Lutetium oxyorthosilicate (LSO) and gadolinium oxyorthosilicate (GSO) crystals are attractive for PET because of their physical characteristics and are increasingly used instead of bismuth germanate (BGO) in PET/CT instrumentation (Table 1). BGO scanners have traditionally been used in the 2-dimensional (2D) mode with interplane septa reducing the amount of scattered radiation in the measurement. To increase sensitivity and shorten imaging protocols, septaless 3-dimensional (3D) data acquisition has replaced 2D acquisition in whole-body imaging. 3D PET is limited mainly by the counting rate capability of the system and the effectiveness of scatter and random coincidence rejection. It has been shown that the use of 3D data acquisition does not affect the diagnostic performance of PET/CT in patients with oncologic diseases (*14,15*). Only a few studies, however, have addressed the role of 3D data imaging in cardiac applications (*16–21*). Figure 1 shows an example of an ^{18}F-FDG patient study at our institution using, sequentially, an LSO-based PET/CT scanner and a conventional BGO PET scanner, demonstrating the excellent image quality provided by the state-of-the-art PET/CT scanner with 3D data acquisition.

Advantages of LSO and GSO scintillators are their relatively fast light decay time and high light yield (*22*). The fast scintillation light decay time decreases dead time and allows the use of short coincidence time windows, thus improving counting rate capability and reducing the contribution of random coincidences. This is reflected in the fact that the counting rate at 50% dead time is ~3.8 times higher in an LSO PET/CT scanner (*23*) than in a 2D BGO scanner (*24*). Typical counting rates in NH_3 scans are measured in the range of 25%–30% dead time in either system, but with a 5–6 times higher counting rate of true coincidences in the LSO system. In addition, high light yield leads to good energy resolution, which results in more effective elimination of radiation scattered within or outside the field of view. Therefore, these materials are well suited to 3D acquisition by increasing the true sensitivity of the scanner and reducing noise from scattered and random coincidences. Because bolus techniques and dynamic image acquisition are used for assessing myocardial perfusion, high counting rate capability is of particular importance (Fig. 2). It has been shown that the input function required for tracer kinetic modeling can be obtained from the time course of activity concentration in the left ventricular blood pool (*25,26*).

The new generation of PET/CT scanners uses smaller crystals, which improve the spatial resolution. In cardiac imaging this plays an important role in minimizing partial-volume effects (*27*). Improving the spatial resolution from 7.0 to 4.5 mm results in about a 30% increase in count recovery based on the average ventricular wall thickness of about 10 mm. Therefore, the use of high-resolution PET

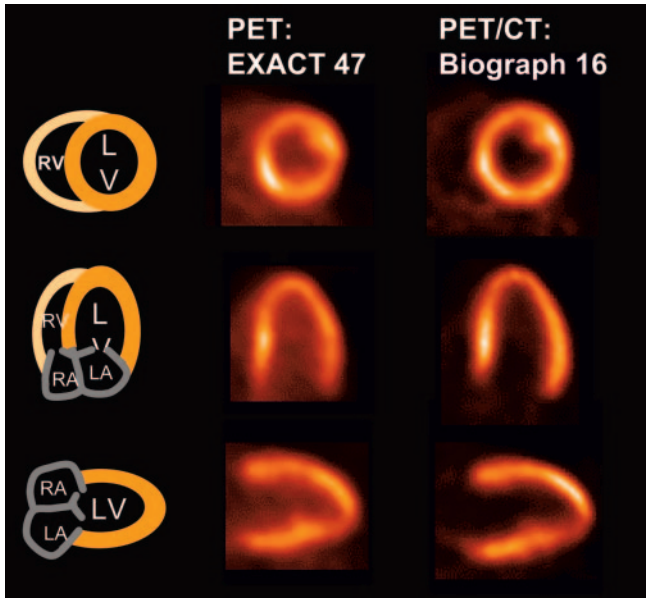

FIGURE 1. Sample ^{18}F-FDG study from our institution in 3D mode with both BGO and LSO as detector material demonstrates the excellent image quality provided by state-of-the-art PET/CT scanners (Biograph 16; Siemens), compared with conventional scanners (EXACT 47; Siemens). LA = left atrium; LV = left ventricle; RA = right atrium; RV = right ventricle.

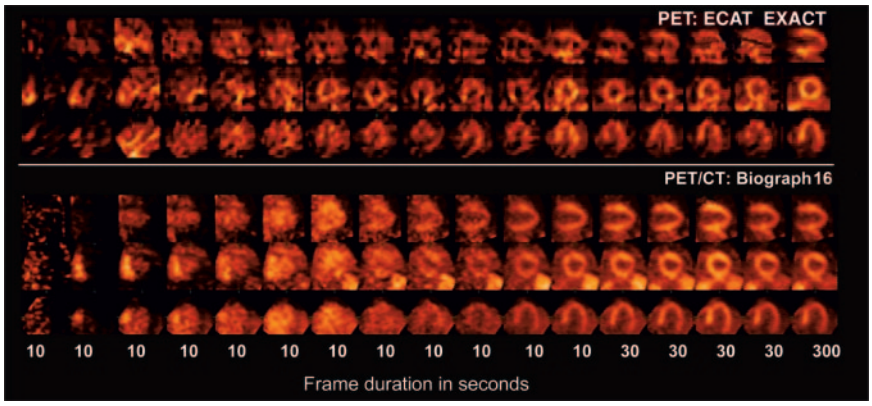

FIGURE 2. Increased sensitivity of LSO-based PET systems is demonstrated in these dynamic series after injection of 555 MBq of ^{13}N ammonia. The 3 top rows show long- and short-axis images of tracer uptake using conventional PET scanner (ECAT EXACT; Siemens). The 3 bottom rows show similar protocol with LSO-based system (Biograph 16; Siemens). Note increased signal-to-noise ratio and improved delineation of cardiac structures during 10-s frames in PET/CT data.

improves the measurement of regional tracer distribution within the myocardium and the quantification of physiologic measurements such as blood flow and metabolism. In addition, high spatial resolution is of utmost importance for the detection of activity within small structures such as the coronary vessel wall. Based on a vessel wall thickness of only about 1–2 mm, the recovery of information requires a high biologic contrast. Assuming a system resolution of 3 mm, which may be available in future PET systems, a target-to-background ratio of 10:1 would be needed to obtain an image contrast of about 2:1. A system resolution of about 10 mm, as currently realized in cardiac SPECT, would require a biologic contrast 10 times higher for an estimated image contrast of 2:1. Therefore, PET appears to be much more promising than SPECT for studying processes in the coronary vessel wall.

Dynamic Data Acquisition

Cardiac PET requires dynamic data acquisition to define tracer kinetics for quantitation of blood flow and metabolism (*28,29*). In addition, cardiac motion effects in the data need to be minimized to improve spatial resolution in the moving heart. Most PET scanners allow electrocardiography gating of the data acquisition in a way similar to that for SPECT. However, for imaging vascular structures, additional respiratory gating may be required to correctly localize vascular activity and to improve the coregistration of PET and CT information (*30,31*). In order to fully exploit the possible dynamic information provided by PET and CT, list-mode acquisition may be the method of choice to retrospectively sort and correlate PET and CT data. Based on list-mode data, several physiologic signals such as electrocardiography and respiration can be used to categorize the information and provide imaging sets recognizing multiple gates (*32*). Figure 3 shows an example of the influence of respiratory gating on cardiac PET images. In this ^{13}N-ammonia PET study, the list-mode data from 2 to 10 min after tracer injection were charted by histogram into 6 respiratory and 2 cardiac gates. The images show end-diastolic frames at end inspiration and at end expiration.

The possibility for retrospective combinations of histogram settings provides another advantage for list-mode acquisition of short-lived isotopes such as ^{82}Rb and ^{15}O-water. Conventional imaging protocols separate dynamic data acquisition from subsequent gated data collection. In list-mode, the entire dataset after a tracer application can be used to generate dynamic images to quantify blood flow. After tracer extraction from the blood, later data can be used to generate any combination of cardiac or respiratory gates.

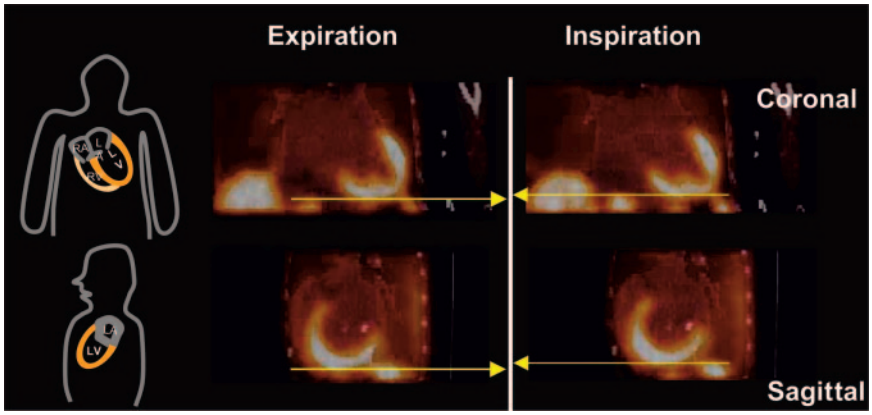

FIGURE 3. Influence of respiratory gating on cardiac motion is demonstrated in this ^{13}N-ammonia study. With acquisition time of 10 min after tracer injection, list-mode data from 2 to 10 min were charted by histogram into 6 respiratory and 2 cardiac cycles. Images show end-diastolic frames in end inspiration and end expiration. Approximated, most apical position in both respiratory states is marked with yellow line. Maximal spatial difference is 8 mm. LA = left atrium; LV = left ventricle; RA = right atrium; RV = right ventricle.

Iterative Reconstruction

PET images are routinely reconstructed using iterative algorithms. The accelerated ordered-subset expectation maximization algorithm with normalization and attenuation weighting has become widely accepted and is routinely used in the clinic (*33*). In 3D mode, scatter can account for more than 50% of the collected counts. Scatter correction can be included in the reconstruction process using, for example, the single scatter simulation method (*34,35*). This scatter model relies on an estimate of the distribution of attenuating media in the field of view—an estimate that can accurately be provided by the CT data. In addition to scatter and AC, the combined PET/CT acquisition of functional and anatomic data may facilitate the incorporation of spatial constraints in the iterative algorithms (*36,37*). The basic assumption is that at positions in which there is a change of tissue type noticeable in CT, chances are high that the activity concentration also changes. Therefore, the reconstruction algorithm allows for larger changes at these positions, reducing the partial-volume effect and enhancing the visibility of small lesions. There are several methods to include the CT information in the PET-image reconstruction, one being the use of smoothed CT data as a weighting factor in statistical image reconstruction (*36*).

CT

With the introduction of electron-beam CT (EBCT) about 30 y ago, fast CT of the heart became possible (*38*). This technology was primarily introduced to measure regional coronary calcification as an early marker of CAD. Although large multicenter studies have been initiated to validate the diagnostic and prognostic value of this approach, EBCT technology has proven to be expensive and of limited usefulness outside cardiac imaging (*39*). The introduction of spiral CT in 1989 represented a major technical breakthrough, offering for the first time continuous-volume CT and hence opening the field of CT angiography (*40*). To increase the imaging volume and, hence, temporal resolution, multislice spiral CT was proposed in 1998. The advantage of multirow detectors is that the table feed per rotation can be increased according to the increased collimated width of the x-ray fanbeam (*12*). The temporal resolution of the system is determined by slice collimation, rotation time, and pitch, where pitch is defined as the ratio of table feed per rotation to the collimated x-ray width (*41*). Currently, multislice CT systems with 16 or 64 slices are recommended for cardiac imaging. The 64-slice systems provide 0.4-mm, nearly isotropic voxel resolution with a rotation time of only 0.33 s. Because noninvasive coronary angiography (i.e., CT angiography) is the most promising cardiac application of multislice CT, imaging parameters need to be optimized to meet the requirements of spatial and temporal resolution. The temporal resolution, defined as time required to acquire the necessary scan data to reconstruct a cardiac CT image, is about 100 ms for EBCT. For multislice CT, temporal resolution is dependent primarily on the time taken by the scanner to complete 1 gantry rotation but can be modified by using partial-scan reconstruction techniques. With these techniques, the image is reconstructed using data acquired from gantry rotations of approximately 240° (180° plus the total detector angle). By using optimized reconstruction algorithms, 180° of data in parallel geometry are extracted from the acquired data and reconstructed, improving the temporal resolution to one half the gantry rotation time. Because the rotation time of the 16-detector-row CT scanner is approximately 400 ms, the resulting temporal resolution is 200 ms. In view of these limitations in temporal resolution, the patient's heart rate becomes an important issue, and most imaging protocols using 16-slice CT applications call for the use of a

TABLE 2
Characteristics and Performance of Commercial PET/CT Systems

Parameter	Biograph 16 (Hi-Rez)	Biograph 64	Gemini GXL	Gemini GXL64	Discovery ST
CT					
Slices	16	64	16	64	16
Rotation speed (s)	0.42	0.33	0.5	0.4	0.5
Temporal resolution (ms)	~105	~90	~120	~100	~120
Spatial resolution (line pairs/cm)	30	30	24	24	15.4
PET					
Scintillator	LSO	LSO	GSO	GSO	BGO
Detector dimensions (mm)	4 × 4 × 25	4 × 4 × 25	4 × 6 × 30	4 × 6 × 30	6.3 × 6.3 × 30
Axial field of view (cm)	16.2	16.2	18	18	15.7
Sensitivity (cps/kBq)	4.5	4.5	8.3	8.3	9.3 (3D)
Peak noise equivalent count rate (kcps)	93	93	70	70	63 (3D)
Transverse resolution (mm)	4.5	4.5	5.2	5.2	6.2 (3D)
Axial resolution (mm)	5.6	5.6	5.5	5.5	7.0 (3D)

Data were obtained from the vendors of the PET/CT systems: Siemens (Biograph 16 and Biograph 64), Philips (Gemini GXL and Gemini GXL64), and GE Healthcare (Discovery ST).

β-blocker to reduce the heart rate to less than 60 beats per minute. However, such acute pharmacologic interventions limit the widespread application of these imaging protocols and may not be required in view of newer multislice CT developments (*42*). A temporal resolution of about 80 ms appears feasible with the newest generation of multislice CT scanners. For a detailed discussion of multislice CT technology, we refer the reader to the reviews of Fuchs et al. (*12*) and Pannu et al. (*43*). Table 2 summarizes the imaging performance of currently available PET/CT instrumentation for cardiac imaging.

AC

The most important aspect of PET/CT is the use of CT information for AC. The effect of attenuation is greater for PET than for SPECT because of coincidence detection of radioactivity—the photon pair associated with an annihilation reaction has to cross the entire body, increasing the likelihood of attenuation. AC for PET is easier to apply, however, because the total attenuation of the pair of detected photons is independent of the origin of the radioactive event within the body. CT images of the chest require only a few seconds using multislice CT instrumentation, and low-dose CT images can be generated with good spatial resolution while minimizing radiation exposure to less than 1 mSv. However, because the attenuation factors for 511 keV have to be extrapolated from low-energy x-ray measurements, conversion factors have to be used for different tissue densities (e.g., heart, lung, and bone). These measurements have been validated in phantom studies and provide accurate measurements of tracer distribution in close agreement with measurements using conventional 511-keV transmission imaging (*44*).

In addition, coregistration of data becomes an important part of AC using CT, because transmission and PET emission data acquisitions are performed separately. The CT acquisition is completed within a few seconds, whereas PET data are collected over several minutes. During the PET acquisition, the influence of respiration is averaged throughout the entire imaging period, whereas the CT image represents only a small part of the respiratory cycle.

Thus, transmission and emission data may be misaligned. This is of great importance because the difference in tissue density between the heart and the surrounding lung is high. Misalignment of emission and transmission data produces artifacts in PET images that may affect the diagnostic performance of the test (Fig. 4) (*45*). Several protocols have been developed to account for these differences in respiratory state, but no standardized protocol for CT transmission scans has yet been developed. Loghin et al. demonstrated, in conventional rest/stress PET studies, that 21.7% of the studies showed misalignment artifacts typically in anterolateral or lateral segments of the left ventricle (*45*). Through manual coregistration of transmission and emission data, the artifacts could be removed.

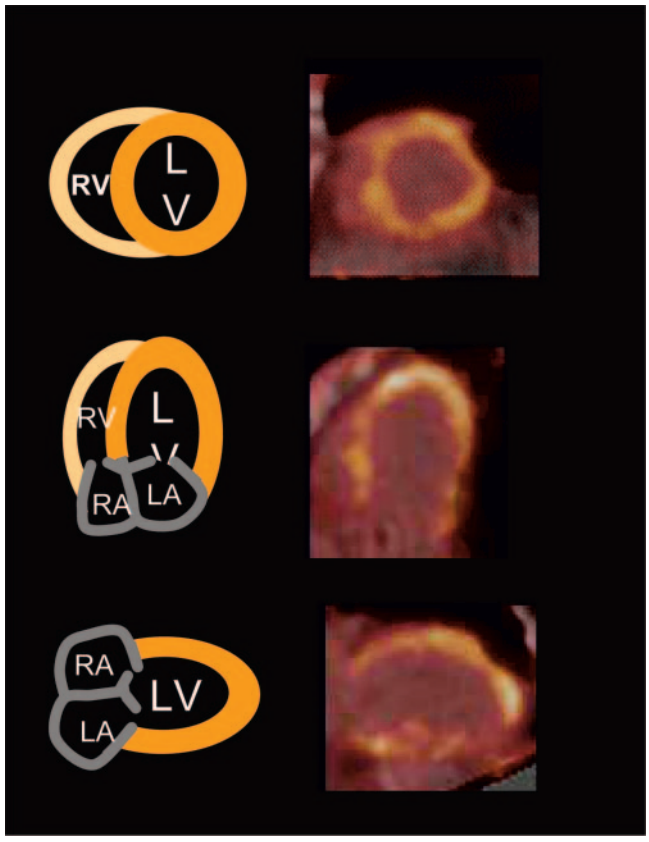

FIGURE 4. Example of PET images attenuation corrected by misaligned CT image with artifacts in anterolateral wall of left ventricle. Artifacts resulted from motion associated with deep breathing of patient during CT scan. Resulting AC map is misaligned with PET emission data. Incorrect AC results in artifactual defects most commonly in anterolateral wall. LA = left atrium; LV = left ventricle; RA = right atrium; RV = right ventricle.

The advantage of CT is the option of repeating scanning before each tracer injection for AC. However, care has to be taken to minimize radiation exposure. The feasibility of CT scans with very low radiation exposures was demonstrated by Koepfli et al. (*46*). These investigators used a PET/CT system that was also equipped with the conventional rotating ^{68}Ge rod sources for transmission. In 7 patients, both conventional and CT-based AC with different tube currents was performed. These data were used for AC of dynamic ^{13}N-ammonia studies. When comparing the myocardial blood flow values using tracer kinetic modeling, no differences for the different CT protocols tested were found. In a second group of 3 patients, consecutive CT scans with tube currents of 10 mA were acquired (corresponding to a radiation dose of as low as 0.05 mSv). Using the different CT scans for AC, the authors again found a high degree of reproducibility of blood flow values. Initial results from our own

group confirmed this finding when using different CT protocols in 20 patients (slow CT: 99 mAs, 120 keV, 46 s; low dose: 20 mAs, 120 keV, 8 s; and ultra low dose: 13 mAs, 80 keV, 5 s). In the same patients, conventional PET was performed shortly after PET/CT (*47*). Relative ^{18}F-FDG uptake was compared in 17 ventricular segments for both conventional PET and PET/CT and did not reveal significant differences for the 3 CT protocols; however, the radiation exposure was drastically different depending on the protocol—0.9, 0.4, and 0.1 mSv, respectively. An increased likelihood of patient motion was observed using the slow CT protocol, introducing artifacts. Although the entire duration of this particular scan was longer (46 s), the CT system is acquiring its slices so quickly that motion is accurately measured instead of being blurred. Taking these first observations into account, a fast, very-low-dose CT scan for AC offers clear advantages for cardiac PET/CT, although further validation is necessary.

COREGISTRATION OF PET AND CT DATA

Because the 2 tomographic data acquisitions are performed in close temporal proximity but not simultaneously, patient motion between scans is likely. In addition, rhythmic cardiac and respiratory motion must be considered. To define the extent of cardiac motion during respiration, several oncology studies have focused on developing standardized breathing protocols for CT data acquisition. Several investigators have studied respiration displacements between PET and CT ranging from 5 to 20 mm (*48,49*). The conclusion of these authors was that coregistration of PET and CT data can be achieved on the order of the spatial resolution of the PET system, which is between 6 and 10 mm. Therefore, respiratory gating appears to be required to improve data coregistration beyond the PET spatial resolution. Using a temperature-sensitive gating device installed in a breathing mask, Boucher et al. described respiratory motion in the axial direction of the cardiac apex of 6.7 ± 3.0 mm (maximal displacement, 11.9 mm) (*30*). Carrasquillo et al. applied respiratory gating using a pneumotachometer in 8 patients. Cardiac ^{18}F-FDG images were reconstructed using CT data acquired at end expiration, end inspiration, and midlevel inspiration (*50*). Regional ^{18}F-FDG uptake varied considerably in the 3 imaging sets. Tracer uptake was found to be most homogeneous at end expiration, whereas the anterior-to-septal and lateral-to-septal ^{18}F-FDG ratios were highest (1.3) at end inspiration.

As an alternative to respiratory gating, software-based coregistration methods may allow for correction of misalignment. In an excellent review, Mäkela et al. defined the achievable accuracy for intra- and intermodal image coregistration (*51*). MRI intramodal alignment can be performed with 1.5- to 3.0-mm limits, whereas PET–PET coregistration results in a 1.0- to 2.5-mm resolution. PET–MRI coregistration is associated with an error of 1.95 ± 1.6 mm. Unfortunately, although these publications indicate its technical feasibility, no commercial implementation for PET/CT cardiac image coregistration is currently available. A complicating factor for cardiac PET/CT coregistration is the fact that myocardial PET emission data are contained in the larger cardiac CT silhouette, which includes ventricles, atria, and large vascular structures.

We therefore investigated an alterative approach to address the transmission–emission misalignment introduced by motion. On the basis of the assumption that tracer uptake defines cardiac tissue, the CT data were iteratively modified (*52*). In the case of a transmission–emission mismatch, CT voxels were added adaptively to match the PET emission data. In 16 patients, rest and stress studies were acquired and polar maps of tracer uptake analyzed. The authors observed in 50% of cases (16/32) modest (<10 mm) and in 28% of cases (9/32) significant (>10 mm) motion artifacts. After applying an emission-driven correction algorithm, a count increase of 8% (modest) and 25% (significant) in the anterior wall and 9% and 16% in the lateral wall was found (Fig. 5). Further validation of this method is required, but it potentially offers a robust and automated approach for emission-based alignment of CT data.

Various software packages exist to allow visualization of cardiac PET and CT data. Each of these applications has been developed in the tradition of the given imaging modality. For example, the polar map has served the nuclear cardiology community well by providing a standardized and widely accepted way of displaying 3D ventricular structures

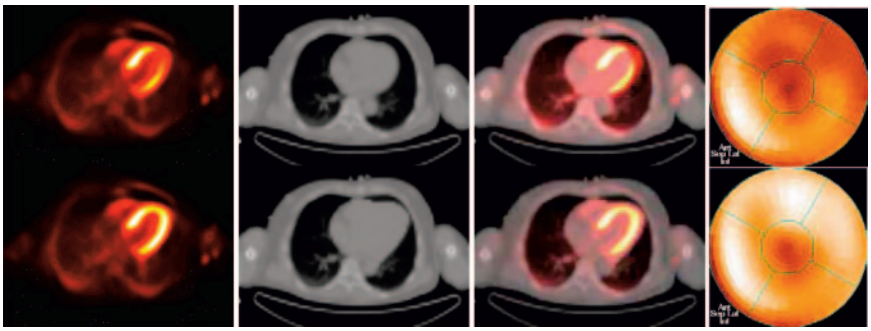

FIGURE 5. Application of emission-driven AC. Initial data showed significant mismatch between PET and CT data used for AC in patient without regional perfusion defects. Apparent reduced tracer uptake in anterolateral segments is clearly visible in fused image display and in polar map (top). On basis of assumption that tracer uptake (even if reduced) can be emitted only from cardiac tissue, attenuation map was modified and image reconstruction repeated, resulting in substantial recovery of tracer uptake. Ant = anterior; Inf = inferior; Lat = lateral; Sep = septal.

in 2 dimensions. Multislice CT also has gained attention by its volume-rendered, realistic, 3D depiction of vascular and cardiac structures. Beyond the existing successful software tools, integrative approaches are needed to interactively show coregistered structural and functional information. The goal is to simultaneously show CT angiography and myocardial perfusion data in a coregistered 3D volume to regionally correlate coronary stenosis with PET perfusion reserve. Coregistration of CT scans for calcification measurements requires only modest modifications, because this information can be derived from standard CT analysis software using thresholds based on Hounsfield units (*53*). Covisualization of PET and CT angiography data is most challenging. In this case, a variety of additional qualitative and quantitative information can be extracted, including morphologic information for coronary arteries (stenosis localization, plaque composition) and global and regional wall motion data (*54*). It is obvious that the visualization of cardiac perfusion, regional function, and coronary anatomy offers an unprecedented combination of noninvasive imaging parameters.

To date, only a few multimodal visualization strategies for PET, SPECT, CT, and MRI have been published. Schindler et al. and Faber et al. manually extracted the coronary arteries from biplanar angiography and combined them with myocardial SPECT perfusion data (*55–57*). This approach automatically warped and projected coronary arteries onto the epicardial surface of the SPECT studies, making use of the a priori information that coronary arteries run along the epicardium.

Aladl et al. recently described an approach for 4-dimensional SPECT–MRI coregistration and fusion (*58*). The MRI wall motion study was segmented on the basis of motion-driven changes in pixel values, essentially removing any static tissue, and subsequently applied mutual-information measures to coregister the datasets. These results were compared with a coregistration performed manually by an expert. Translational differences were found on the order of 1 mm with MRI segmentation and 4 mm without. This technique can be applied to PET/CT data as well and offers a high degree of automation. For visualization, Aladl used a conventional fused display to blend morphologic and functional image information both in static views and in cine mode, because both modalities provided gated datasets. In a very recent study, ^{13}N-ammonia PET uptake values were mapped onto the endocardial surface of a 3D CT volume-rendered angiogram after manually segmenting the cardiac structures on the CT scan (*59*). This technique allows for elegant covisualization of the coronary arteries and the functional PET information using volume-rendering techniques.

We propose a new way of integrating PET and CT data (Fig. 6) (*60*). Instead of using a conventional fusion display, which may hide information if both PET and CT show a bright signal, we segment the left ventricular wall on the basis of CT data and color code it with the original or parametric PET information. This approach essentially allows the cardiac wall to be mapped with a variety of qualitative and quantitative data such as tracer uptake, myocardial blood flow (as a result of kinetic modeling), or even

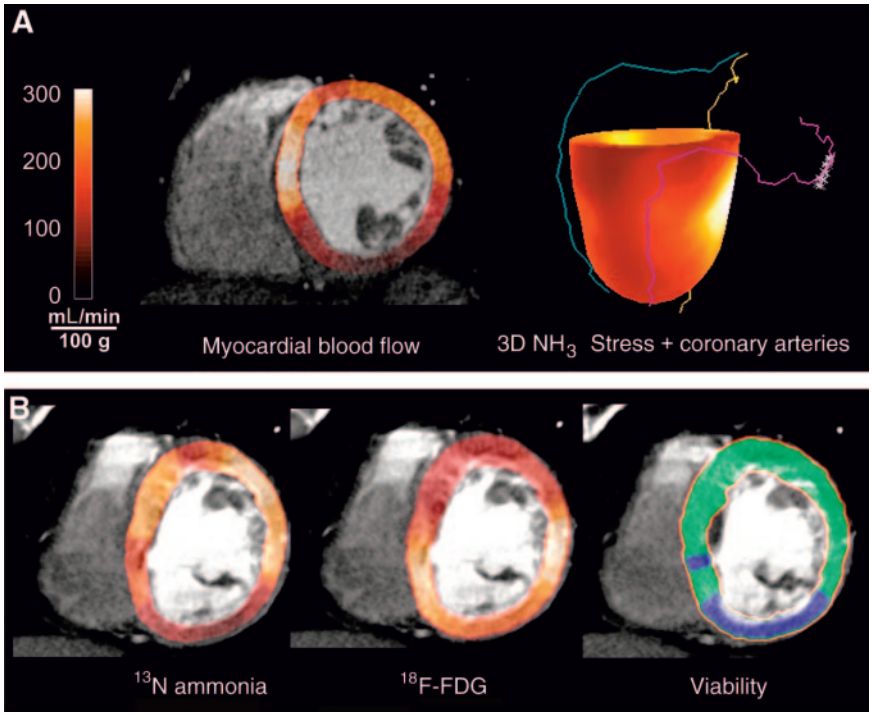

FIGURE 6. (A) Visualization of CT angiography (CTA) and PET data requires integrative display format. Myocardial blood flow under stress conditions with ^{13}N ammonia was calculated using dynamic data. These regional flow values were mapped in color code onto segmented wall from coronary angiography study. In addition, coronary tree was manually extracted and superimposed on 3D polar map of myocardial blood flow. (B) ^{13}N-ammonia and ^{18}F-FDG retention from viability examination were mapped onto myocardial wall. The combination of these 2 tracer studies provides tissue classification, which can be used to describe myocardium specifically. Blue = mismatch or hibernating myocardium; green = normal; LV = left ventricle; RCA = right coronary artery; RV = right ventricle.

tissue viability classification, integrating several independent information sets (e.g., mismatch of flow and metabolism).

RADIATION EXPOSURE

Radiation exposure from a PET/CT study is the sum of the effective dose from the incorporated radiotracer and the dose from external x-ray irradiation during the selected CT-acquisition protocol.

For a 370-MBq ^{18}F-FDG injection, the effective dose is 7 mSv. For rest–stress ^{13}N-ammonia (2 × 550 MBq) or ^{82}Rb (2 × 1,500 MBq), the effective doses are 2.2 mSv and 5.0 mSv, respectively (*61*).

The effective dose per CT examination depends on the acquisition parameters chosen (kV, mAs) and the body region being scanned. Measurements of radiation exposure in oncologic whole-body ^{18}F-FDG PET/CT examinations (*62*) showed an effective dose of 14–18 mSv from the contrast-enhanced diagnostic CT scan covering the whole body. Reducing radiation exposure by limiting the axial field of view or changing the CT tube current according to anatomy has been proposed to reduce radiation exposure by up to 30%–40% (*11*). Table 3 summarizes estimates of radiation exposures for different cardiac multislice CT and EBCT protocols. More recently, electrocardiography-related tube current modulation was introduced for coronary artery calcium scoring. This protocol leads to a very low radiation exposure of 0.72 MSv (*63*).

CLINICAL APPLICATIONS

Diagnosis of CAD

With the changing pathophysiologic understanding about CAD, it is becoming increasingly difficult to define the gold standard for disease detection. Conventionally, the presence of 50%–75% coronary stenosis is considered indicative of obstructive CAD. However, evidence is increasing that although the degree of stenosis may be related to the presence or absence of symptoms, the prognosis of patients cannot be predicted on the basis of angiographic criteria (*5*). A study has shown that a large subset of patients with acute myocardial infarction has coronary culprit lesions of less than 50% narrowing, limiting the use of the degree of stenosis as a predictor for acute ischemic syndromes (*64*). A consensus exists that indications for revascularization in patients with stable coronary disease should be based on evidence of myocardial ischemia (*65*). In symptomatic and asymptomatic patients with CAD, a large body of data indicates that the prognosis depends on the extent and severity of perfusion abnormalities during stress interventions (*4,5*). Therefore, the strategy of revascularization is aimed at reducing the individual risk to patients demonstrating a significant amount of ischemic myocardium at risk. On the other hand, in noninvasive tests such as MPI, the demonstration of normal results during maximal physical or pharmacologic stress is associated with a very low risk of cardiovascular complications (*4*). Therefore, the therapeutic management of patients with known CAD is based on functional characterization of the disease process. The combination of scintigraphic measurement of perfusion and CT depiction of coronary morphology may increase the accuracy of linking functional and morphologic data. This combination is expected to decrease the need for diagnostic cardiac catheterization and prove to be the method of choice for selecting patients for therapeutic intervention.

TABLE 3
Effective Radiation Dose for Cardiac PET/CT Studies (*61,123,124*)

Study	Effective radiation dose (mSv)
PET	
^{18}F-FDG (370 MBq)	7.0
^{13}N-NH3 rest/stress (2 × 550 MBq)	2.2
^{82}Rb rest/stress (2 × 740 MBq)	5.0
$H_2{}^{15}O$ rest/stress (2 × 740 MBq)	1.4
Transmission ^{68}Ge rod sources	0.08–0.13
Multislice CT	
Calcium scoring	1.5–6.2
CT angiography	6.7–13.0
CT-based PET attenuation correction	0.23–5.66

Noninvasive Coronary Angiography by CT Angiography

A large number of studies have recently been published demonstrating the increasing accuracy of multislice-CT angiography for the detection of CAD. With the availability of 16- and 64-slice scanners, the sensitivity and specificity for detection of significant coronary artery stenosis are exceeding 90% (*43,66,67*). Most investigators using 16-slice CT have recommended the use of β-blockers to reduce heart rate and, thus, the incidence of motion artifacts. With the introduction of the 64-slice CT scanner, the need to apply β-receptor blockade appears to be less critical (*42*). First experiences with the 64-slice CT scanner indicate that coronary arteries with a diameter of >1.5 mm can be evaluated without exclusion. Leschka et al. reported that none of the coronary segments of 67 consecutive patients needed to be excluded from analysis (*42*). CT correctly identified all 20 patients without significant stenoses on invasive angiography. Overall, sensitivity for classifying stenosis was 94%, specificity was 97%, positive predictive value was 87%, and negative predictive value was 99%. These results represent a significant improvement over the previous generations of multislice CT instrumentation. Using 4- to 8-slice CT, a sensitivity of 58%–86% for detection of coronary stenosis has been reported, but up to 32% of the vessels had to be excluded from analysis because of limited image quality. Using 16-slice CT, overall sensitivity, including all segments, was reported to range from 73% to 95% depending on the diameter of the segments, the mode of analysis, and

the patient selection criteria (*67,68*). However, in some studies the evaluation was limited to branches having a diameter of >2 mm. Most studies were a single-center evaluation and involved patient populations with a high prevalence of CAD. Further prospective multicenter studies are needed to confirm the high diagnostic value of multislice CT imaging for the detection of CAD (*69*).

Multislice CT technology is expected to stabilize, resulting in longer product cycles and thus allowing for a more in-depth validation of this technology. However, there is little question that noninvasive coronary angiography will become a clinical reality, changing the workup of patients suspected of having obstructive CAD and the follow-up after surgical and percutaneous revascularization (*70*).

A drawback of CT angiography is its limited ability to correctly assess regional coronary stenosis in the presence of severe coronary calcification. Leschka et al., in their first evaluation of the 64-slice CT scanner, reported that coronary calcification was present in 18% of all coronary branches, resulting in beam-hardening artifacts and decreased visualization of the coronary lumen (*42*). Calcium deposits were responsible for most false-negative and all 24 false-positive results. However, all false-positive lesions showed coronary wall irregularities on invasive coronary angiography. Again, the use of MPI at the time of CT angiography may help to reduce the number of false-positive results, because normal perfusion reserve in segments distal to a coronary calcification may rule out a high-grade lesion. Berman et al., in a recent publication, demonstrated that only about 30% of patients with severe coronary artery calcification (Agatston score > 1,000) had stress perfusion defects (*71*).

Assessment of Blood Flow

The advantage of using PET in combination with CT to assess myocardial blood flow is the availability of tracers with a very short physical half-life, reducing the radiation dose and shortening the test.

^{15}O-Water has a physical half-life of only 120 s and suitable tracer kinetics for the evaluation of myocardial blood flow. Because ^{15}O-water is freely diffusible, the myocardial tracer uptake is linearly related to myocardial blood flow (*72,73*). However, because of its rapid kinetics, dynamic data acquisition is necessary to delineate the washing in and out of the tracer as a marker of myocardial perfusion. ^{82}Rb has physiologic characteristics similar to those of ^{99m}Tc-labeled blood flow markers (*74*). In addition, its short half-life of 76 s allows the determination of rest and stress perfusion studies within 30 min. Several PET studies using ^{82}Rb as a blood flow marker have shown diagnostic accuracy higher than that of invasive procedures and SPECT perfusion imaging (Table 4). ^{82}Rb is a generator-derived radiopharmaceutical and, thus, does not require an on-site cyclotron for radioisotope production. Therefore, this radiopharmaceutical appears to be practical for the evaluation of rest and stress perfusion using PET/CT instrumentation (*75*). ^{15}O-Water may be more suitable for quantitative blood flow measurements but still has to be considered experimental. An alternative tracer of blood flow is ^{13}N-ammonia, which has a 10-min physical half-life but requires an on-site cyclotron for production. This tracer provides excellent image quality and has been validated extensively, demonstrating high diagnostic and prognostic accuracy for detection of CAD (*76,77*). Thus, qualitative and quantitative data on regional myocardial perfusion can be derived, and parameters such as coronary flow reserve and coronary vascular resistance can be determined (*77,78*).

TABLE 4
Diagnostic Performance of PET-Flow Determinations

Study	*n*	Sensitivity (%)	Specificity (%)
^{13}N-ammonia			
Schelbert (*125*)	45	98	100
Tamaki (*126*)	51	98	100
Muzik (*127*)	35	87	96
^{82}Rb			
Go (*128*)	202	93	78
Stewart (*129*)	81	83	86
Grover-McKay (*130*)	31	100	13
Marwick (*131*)	74	90	100

Although PET has been well validated for detection of obstructive CAD, relatively few publications have documented the diagnostic superiority of PET in direct comparison with SPECT. Balanced CAD can be detected only by measuring regional flow reserve (*75*). PET appears to be more sensitive than SPECT for characterizing local stenosis and defining the extent of vascular impairment. Yoshinaga et al. demonstrated that abnormalities associated with coronary artery stenosis (<50%) were identified more frequently with PET flow reserve measurements than with SPECT (*79*). Future studies have to address the question of whether the higher diagnostic accuracy of PET, combined with the more rapid patient throughput, compensates for its higher cost and greater logistic infrastructure requirements. First experiences with ^{82}Rb suggest a potential role for PET in the work-up of patients with suspected or proven CAD (*80*).

Early Detection of CAD

Risk factor analysis and epidemiologic models based on the populations of the Framingham or PROCAM (Prospective Cardiovascular Münster) studies may allow individual risk assessment (*81,82*). Despite this sophisticated calculation of individual risk based on genetic and environmental risk factors, the accuracy of predicting acute myocardial infarction in an individual patient remains relatively low (*83*). Therefore, the need to develop additional biomarkers for the existence of CAD is of great importance. First results evaluating the presence of coronary calcification as incremental information in individual risk assessment are emerg-

ing. Pletcher et al. recently published a metaanalysis that demonstrated an adjusted relative risk of 2.1 (95% confidence interval, 1.6–2.9) for a coronary calcium score of 1–100. Relative risk estimates for higher scores ranged from 3.0 to 17.0. The authors concluded that coronary calcification is an independent predictor of a CAD event (*84*). Greenland et al., in a prospective observational study comparing Framingham risk score with coronary calcification score in 1,461 asymptomatic adults, recently showed that a high coronary calcification score can modify predicted risk based on Framingham risk score alone, especially among patients in the intermediate-risk category, for whom clinical decision making is most important (*85*). Shaw et al. recently demonstrated that the degree of coronary calcification measured by the Agatston score can identify patients with differing risk profiles (*86*).

A cohort of 10,377 asymptomatic individuals was followed for a mean of 5 y. The death rate was 2.4%. In a risk-adjusted model, coronary calcification score was an independent predictor of mortality. This observational study strongly suggested that coronary calcification score depicted by EBCT or multislice CT provides incremental prognostic information (*86*). Several prospective studies are currently under way to further investigate the prognostic value of coronary calcification score. Raggi et al. demonstrated that the absence of coronary calcification in a subgroup of diabetic patients was associated with an incidence of cardiac events comparable to that in nondiabetics without coronary calcification. On the other hand, in the diabetic population the risk was increased at each coronary calcification score level (*87*). Two studies have compared coronary calcification score and stress-induced perfusion abnormalities in asymptomatic adults (*71,88*). Anand et al. (*88*) observed a high prevalence of silent ischemia based on MPI in 18% of individuals with a coronary calcification score of 100–400. Patients with a coronary calcification score of >400 showed abnormal MPI in 45% of the cases. In contrast to these results, other studies suggest a lower incidence of MPI abnormalities associated with coronary calcification. Berman et al. (*71*) emphasize that normal MPI is often associated with significant coronary calcification. These investigators identified moderate and large stress perfusion defects (<10% of the left ventricle) in less than 10% of 1,195 asymptomatic patients with a coronary calcification score of <1,000. This finding implies a potential role for measuring coronary calcification before MPI to increase the sensitivity for diagnosing early nonobstructive CAD (*71*). Relative myocardial perfusion changes detectable by SPECT occur predominantly in advanced CAD with stenosis < 50%, whereas PET findings for coronary flow reserve may be abnormal in patients at risk for development of CAD. Several PET studies have documented a reduced myocardial flow reserve associated with risk factors such as hypercholesterolemia, diabetes mellitus, hypertension, and smoking (*89–91*). The use of endothelial dysfunction as a possible biomarker for active CAD is further supported by the notion that inflammatory processes not only are present in the area of plaque rupture but also involve much larger parts of the coronary vascular tree (*92*). The hypothesis of more widespread inflammatory changes in patients with acute coronary syndromes may also explain the observed impaired coronary flow reserve measurements in remote vascular territories of patients with acute myocardial infarction (*93*). Therefore, it is likely that the combination of coronary calcification and myocardial flow reserve measurements by PET may further enhance the management of individuals at risk of premature CAD. Relatively few data have been published defining the prognostic value of absolute flow reserve measurements as a marker of endothelial dysfunction. However, reports by Schachinger et al., Schindler et al., and Halcox et al. indicate that patients with impaired coronary vascular reactivity (determined invasively and noninvasively) have a worse prognosis than patients with a normal coronary response pattern (*94–96*). Several studies have indicated that the coronary flow reserve can be improved by lipid-lowering medication and other pharmacologic treatments (*97–99*). Quantitative evaluation of flow reserve or vascular reactivity may serve as an important surrogate endpoint for preventive therapeutic strategies. It is expected that this potential role will be broadened by combining PET and CT information. The time course of CAD progression or regression based on changes of calcification, soft-plaque formation, and endothelial function can be noninvasively defined and may serve as a comprehensive endpoint in the evaluation of new and established therapies (*97,100–102*).

Identifying Plaque Burden

Coronary calcification is one of the first biomarkers identifying atherosclerotic coronary lesions. However, several studies indicate that even in the absence of coronary calcification, plaques can be detected by CT, MRI, or ultrasound measurements (*103–105*). A recent study comparing CT with intravascular ultrasound revealed a 19% incidence of noncalcified lesions. There are no data indicating whether calcified or noncalcified lesions are more likely to rupture during an acute ischemic event. However, the increasing spatial resolution of multislice CT may allow the detection of vascular alterations in the form of calcified and noncalcified plaques. Becker et al. recently characterized various plaque subtypes using density measurements (Hounsfield units) (*106*). With the advent of molecular imaging, there may be an opportunity to enhance contrast in plaque imaging by combining scintigraphic data with CT characterization of individual plaques. The first application of this approach was provided by Rudd et al. (*107*), who observed higher ^{18}F-FDG uptake in patients with symptomatic carotid lesions than in asymptomatic patients. Colocalization of ^{18}F-FDG was observed in cells surrounding the lipid core near the fibrous cup of the plaque. These data suggest that

it may be possible to identify the inflammatory component of atherosclerotic plaques in vivo, thereby allowing the biologic activity within plaques to be studied. However, ^{18}F-FDG represents a relatively nonspecific marker for molecular processes. New radiopharmaceuticals that target the extracellular matrix proteinases or proteins that are upregulated during the inflammatory process may be of interest (*108,109*). First data using matrix proteinase inhibitors, as shown by Schafers et al. (*108*), indicate specific uptake of this tracer in a transgenic mouse model with atherosclerotic plaques. Other studies have indicated that radiolabeled annexin V can be used to identify apoptosis in macrophages infiltrating the plaque during the inflammatory phase (*110,111*). In addition, several adhesion molecules have been proposed as possible targets (*112*). The question remains as to whether the sensitivity and spatial resolution of PET/CT will allow an accurate coregistration of biologic and morphologic data to specifically delineate the inflammatory process involving coronary arteries. We recently introduced a radiopharmaceutical that targets exposed collagen after plaque rupture (*113*). Again, data in the APoE −/− transgenic mouse model indicate high tracer uptake in the areas of plaque rupture induced by wire ablation. In addition to the imaging of inflammatory components of plaque, imaging of thrombus deposition, which may be an early indicator of the development of acute ischemic syndromes, may be possible. Peptides targeting fibrin may be suitable for detecting the initiation of thrombus formation in patients with unstable CAD (*114*). These applications of molecular imaging for plaque characterization are in the early phases of preclinical evaluation. However, with the introduction of PET/CT, such experimental approaches can be transferred to the clinical environment and supported by the coregistration of CT and PET images. In addition to the evaluation of plaque biology, clinical data are needed to validate the prognostic value of such molecular imaging approaches. There is no question that PET/CT images will improve the evaluation of molecular signals, because targeted tracer signals require anatomic information. Future studies will have to show, however, whether PET/CT can show biologic signals in the beating heart and provide incremental prognostic information.

Assessment of Heart Failure

The results of multicenter trials on patients with heart failure indicate that up to 50% of patients with impaired left ventricular function have CAD (*115*). Because the treatment strategies for patients with CAD are different from those for patients with primary myocardial disease, such as dilated cardiomyopathy, accurate differentiation of ischemic and nonischemic heart disease is important. Again, with the advent of noninvasive coronary angiography by CT, the combination of PET and CT may help not only to separate patients with and without CAD but also to define the extent of reversible and irreversible ventricular dysfunction based on metabolic evaluation of the left ventricular myocardium (Fig. 6B). There are relatively few data available demonstrating the accuracy of CT angiography in patients with impaired left ventricular function. The quality of the contrast bolus in patients with low cardiac output may impair image quality. However, because of the reduced cardiac function, motion artifacts may be less prevalent in this population. Therefore, the newer generation of multislice CT scanners is expected to make possible the accurate detection of CAD in patients with impaired left ventricular function. PET has been validated extensively in the assessment of tissue viability using the combination of metabolic imaging with ^{18}F-FDG and evaluation of myocardial blood flow. The extent of tissue viability predicts recovery of left ventricular function after revascularization (*116*). Based on coronary angiographic data provided by CT angiography and by the assessment of tissue viability, a noninvasive diagnostic workup may be possible. This possibility may be especially important for patients being considered for cardiac transplantation, when information about the viability of residual tissue and the extent of CAD, as defined by CT angiography, helps with the decision-making process.

The presence of mismatch between flow and metabolism is of high prognostic value (*2,117,118*). Several studies have indicated that the presence of metabolic activity in segments with severe dysfunction is associated with higher risk if these segments are not revascularized (*118,119*). A study has also shown that residual viability in dysfunctional myocardium is associated with less perioperative risk from the revascularization (*120*). Therefore, the combination of PET/CT in patients with severe left ventricular dysfunction may improve the diagnostic process and help avoid unnecessary invasive procedures. This comprehensive cardiac evaluation with PET/CT includes not only the CT angiography data and the myocardial tissue characterization but also the assessment of regional function through left ventricular ejection fraction (*121*). Therefore, with a single, noninvasive imaging procedure, the extent and severity of left ventricular dysfunction, the extent of tissue viability, and the overall extent of CAD can be characterized and used to risk-stratify the patient.

Besides being useful for the clinical characterization of patients with left ventricular dysfunction, PET/CT may be attractive for clinical research. This imaging modality provides surrogate endpoints for interventional studies, especially in the application of gene or cell therapy, which requires regional delineation of therapeutic interventions. Studies using reporter gene imaging have shown that the regional effects of gene therapy can be measured with tracer techniques such as PET/CT (*122*).

CONCLUSION

The clinical success of PET/CT as an imaging modality that combines structure and metabolism has been driven by

TABLE 5
Comparison of Diagnostic Information Provided by PET and Multislice CT

Parameter	PET	Multislice CT
Left ventricular function	++	+++
Coronary calcification	−	++
Coronary angiography	−	++
Perfusion	+++	+
Metabolism	+++	−
Viability	+++	+ (?)
Plaque morphology	−	+
Molecular imaging	++	−

its increasing acceptance in oncology. PET/CT is expected to emerge as the method of choice for staging and therapy control of oncology patients. On the other hand, multislice CT technology is rapidly approaching the goal of allowing coronary angiography to be performed noninvasively. With the ability to characterize coronary lesion severity at a level of diagnostic accuracy similar to that of invasive coronary angiography, the close correlation of plaque morphology with functional measurements such as myocardial perfusion will be increasingly appreciated. Furthermore, early detection of CAD will be improved by the use of detailed structural and molecular information provided by PET/CT. For example, coronary calcification measurements combined with specific tracer techniques for the characterization of inflammatory processes may help to identify patients who are at high risk for the development of acute ischemic syndromes. Tracer techniques will continue to be of use for the characterization of myocardial tissue viability in patients with advanced CAD and heart failure and may also be applied to monitor new metabolic therapy strategies. The combination of CT morphology and PET perfusion may serve as a surrogate endpoint in new drug evaluations aimed at reversing CAD. The clinical impact of PET/CT and other multimodality instrumentation remains to be defined. We have speculated on future clinical applications in cardiology, but only direct comparison with other cardiac imaging modalities will define its future role (Table 5). The imaging and cardiology communities have to define new diagnostic strategies to integrate the multiplicity of information provided by multimodal imaging approaches. The question of whether hardware or software fusion of information will be the most appropriate strategy is currently open. Cost, product availability, ownership, reimbursement, and patient-referral patterns will be important factors defining the future use of PET/CT in cardiology. The necessary validation studies represent an exciting challenge for nuclear cardiology but also require the development of interdisciplinary imaging groups to integrate the expertise necessary to exploit the diagnostic potential of PET/CT.

ACKNOWLEDGMENTS

The excellent secretarial support of Gabriele Sonoda, Sigrid Matussek, and Birgit Meissner is well appreciated. The authors thank David McElroy for his editorial assistance.

REFERENCES

1. Gould KL, Schelbert HR, Phelps ME, Hoffman EJ. Noninvasive assessment of coronary stenoses with myocardial perfusion imaging during pharmacologic coronary vasodilatation. V. Detection of 47 percent diameter coronary stenosis with intravenous nitrogen-13 ammonia and emission-computed tomography in intact dogs. *Am J Cardiol.* 1979;43:200–208.
2. Schwaiger M, Melin J. Cardiological applications of nuclear medicine. *Lancet.* 1999;354:661–666.
3. Ladenheim ML, Pollock BH, Rozanski A, et al. Extent and severity of myocardial hypoperfusion as predictors of prognosis in patients with suspected coronary artery disease. *J Am Coll Cardiol.* 1986;7:464–471.
4. Iskandrian AS, Chae SC, Heo J, Stanberry CD, Wasserleben V, Cave V. Independent and incremental prognostic value of exercise single-photon emission computed tomographic (SPECT) thallium imaging in coronary artery disease. *J Am Coll Cardiol.* 1993;22:665–670.
5. Hachamovitch R, Hayes SW, Friedman JD, Cohen I, Berman DS. Stress myocardial perfusion single-photon emission computed tomography is clinically effective and cost effective in risk stratification of patients with a high likelihood of coronary artery disease (CAD) but no known CAD. *J Am Coll Cardiol.* 2004;43:200–208.
6. Melon PG, Beanlands RS, DeGrado TR, Nguyen N, Petry NA, Schwaiger M. Comparison of technetium-99m sestamibi and thallium-201 retention characteristics in canine myocardium. *J Am Coll Cardiol.* 1992;20:1277–1283.
7. Ficaro EP, Fessler JA, Shreve PD, Kritzman JN, Rose PA, Corbett JR. Simultaneous transmission/emission myocardial perfusion tomography: diagnostic accuracy of attenuation-corrected ^{99m}Tc-sestamibi single-photon emission computed tomography. *Circulation.* 1996;93:463–473.
8. Matsunari I, Boning G, Ziegler SI, et al. Attenuation-corrected rest thallium-201/stress technetium 99m sestamibi myocardial SPECT in normals. *J Nucl Cardiol.* 1998;5:48–55.
9. Hendel RC. Attenuation correction: eternal dilemma or real improvement? *Q J Nucl Med Mol Imaging.* 2005;49:30–42.
10. Townsend DW, Cherry SR. Combining anatomy and function: the path to true image fusion. *Eur Radiol.* 2001;11:1968–1974.
11. Kalender WA, Wolf H, Suess C. Dose reduction in CT by anatomically adapted tube current modulation. II. Phantom measurements. *Med Phys.* 1999;26:2248–2253.
12. Fuchs T, Kachelriess M, Kalender WA. Technical advances in multi-slice spiral CT. *Eur J Radiol.* 2000;36:69–73.
13. Lardinois D, Weder W, Hany TF, et al. Staging of non-small-cell lung cancer with integrated positron-emission tomography and computed tomography. *N Engl J Med.* 2003;348:2500–2507.
14. Lartizien C, Kinahan PE, Comtat C. A lesion detection observer study comparing 2-dimensional versus fully 3-dimensional whole-body PET imaging protocols. *J Nucl Med.* 2004;45:714–723.
15. Halpern BS, Dahlbom M, Quon A, et al. Impact of patient weight and emission scan duration on PET/CT image quality and lesion detectability. *J Nucl Med.* 2004;45:797–801.
16. Schafers KP, Spinks TJ, Camici PG, et al. Absolute quantification of myocardial blood flow with $H_2{}^{15}O$ and 3-dimensional PET: an experimental validation. *J Nucl Med.* 2002;43:1031–1040.
17. Lubberink M, Boellaard R, van der Weerdt AP, Visser FC, Lammertsma AA. Quantitative comparison of analytic and iterative reconstruction methods in 2- and 3-dimensional dynamic cardiac ^{18}F-FDG PET. *J Nucl Med.* 2004;45:2008–2015.
18. Knesaurek K, Machac J, Krynyckyi BR, Almeida OD. Comparison of 2-dimensional and 3-dimensional ^{82}Rb myocardial perfusion PET imaging. *J Nucl Med.* 2003;44:1350–1356.
19. Votaw JR, White M. Comparison of 2-dimensional and 3-dimensional cardiac ^{82}Rb PET studies. *J Nucl Med.* 2001;42:701–706.
20. Brogsitter C, Gruning T, Weise R, et al. ^{18}F-FDG PET for detecting myocardial viability: validation of 3D data acquisition. *J Nucl Med.* 2005;46:19–24.
21. Brink I, Schumacher T, Talazko J, et al. 3D-cardiac-PET: a recommendable clinical alternative to 2D-cardiac-PET? *Clin Positron Imaging.* 1999;2:191–196.

22. Humm JL, Rosenfeld A, Del Guerra A. From PET detectors to PET scanners. *Eur J Nucl Med Mol Imaging.* 2003;30:1574–1597.
23. Martinez Canet M, Bercier Y, Schwaiger M, Ziegler S. Improved performance of a PET/CT tomograph after electronics upgrade [abstract]. *J Nucl Med.* 2005;46(suppl):488P.
24. Brix G, Zaers J, Adam LE, et al. Performance evaluation of a whole-body PET scanner using the NEMA protocol: National Electrical Manufacturers Association. *J Nucl Med.* 1997;38:1614–1623.
25. Yoshida K, Endo M, Fukuda H, et al. Measurement of arterial tracer concentrations from cardiac PET images. *J Comput Assist Tomogr.* 1995;19:182–187.
26. Raylman RR, Caraher JM, Hutchins GD. Sampling requirements for dynamic cardiac PET studies using image-derived input functions. *J Nucl Med.* 1993;34: 440–447.
27. Parodi O, Schelbert HR, Schwaiger M, Hansen H, Selin C, Hoffman EJ. Cardiac emission computed tomography: underestimation of regional tracer concentrations due to wall motion abnormalities. *J Comput Assist Tomogr.* 1984;8:1083–1092.
28. Hutchins GD, Schwaiger M, Rosenspire KC, Krivokapich J, Schelbert H, Kuhl DE. Noninvasive quantification of regional blood flow in the human heart using N-13 ammonia and dynamic positron emission tomographic imaging. *J Am Coll Cardiol.* 1990;15:1032–1042.
29. vom Dahl J, Muzik O, Wolfe ER Jr, Allman C, Hutchins G, Schwaiger M. Myocardial rubidium-82 tissue kinetics assessed by dynamic positron emission tomography as a marker of myocardial cell membrane integrity and viability. *Circulation.* 1996;93:238–245.
30. Boucher L, Rodrigue S, Lecomte R, Benard F. Respiratory gating for 3-dimensional PET of the thorax: feasibility and initial results. *J Nucl Med.* 2004;45: 214–219.
31. Visvikis D, Lamare F, Turzo A, et al. Efficiency of respiratory gating for motion correction in PET [abstract]. *J Nucl Med.* 2005;46(suppl):163P.
32. Nekolla S, Martinez M-J, Howe F, Kehren F, Ziegler S. Integrating cardiac PET/CT list mode acquisition in a clinical routine environment: implementation and initial experiences [abstract]. *J Nucl Cardiol.* 2005;12(suppl):S65.
33. Boellaard R, van Lingen A, Lammertsma AA. Experimental and clinical evaluation of iterative reconstruction (OSEM) in dynamic PET: quantitative characteristics and effects on kinetic modeling. *J Nucl Med.* 2001;42:808–817.
34. Ollinger JM. Model-based scatter correction for fully 3D PET. *Phys Med Biol.* 1996;41:153–176.
35. Watson C, Newport D, Casey M, deKemp R, Beanlands R, Schmand M. Evaluation of simulation-based scatter correction for 3-D PET cardiac imaging. *Nuclear Science IEEE Transactions OM.* 1997;44:90–97.
36. Comtat C, Kinahan PE, Fessler JA, et al. Clinically feasible reconstruction of 3D whole-body PET/CT data using blurred anatomical labels. *Phys Med Biol.* 2002;47:1–20.
37. Gindi G, Lee M, Rangarajan A, Zubal IG. Bayesian reconstruction of functional images using anatomical information as priors. *IEEE Trans Med Imaging.* 1993;12:670–680.
38. Budoff MJ, Brundage BH. Electron beam computed tomography: screening for coronary artery disease. *Clin Cardiol.* 1999;22:554–558.
39. Nasir K, Budoff MJ, Post WS, et al. Electron beam CT versus helical CT scans for assessing coronary calcification: current utility and future directions. *Am Heart J.* 2003;146:969–977.
40. Kalender WA, Seissler W, Klotz E, Vock P. Spiral volumetric CT with single-breath-hold technique, continuous transport, and continuous scanner rotation. *Radiology.* 1990;176:181–183.
41. Part 2–44: particular requirements for the safety of x-ray equipment for computed tomography. In: *Medical Electrical Equipment.* Geneva, Switzerland: International Electrotechnical Commission; 1999.
42. Leschka S, Alkadhi H, Plass A, et al. Accuracy of MSCT coronary angiography with 64-slice technology: first experience. *Eur Heart J.* 2005;26:1482–1487.
43. Pannu HK, Flohr TG, Corl FM, Fishman EK. Current concepts in multi-detector row CT evaluation of the coronary arteries: principles, techniques, and anatomy. *Radiographics.* 2003;23(suppl):S111–S125.
44. Kinahan PE, Townsend DW, Beyer T, Sashin D. Attenuation correction for a combined 3D PET/CT scanner. *Med Phys.* 1998;25:2046–2053.
45. Loghin C, Sdringola S, Gould KL. Common artifacts in PET myocardial perfusion images due to attenuation-emission misregistration: clinical significance, causes, and solutions. *J Nucl Med.* 2004;45:1029–1039.
46. Koepfli P, Hany TF, Wyss CA, et al. CT attenuation correction for myocardial perfusion quantification using a PET/CT hybrid scanner. *J Nucl Med.* 2004;45: 537–542.
47. Souvatzoglou M, Bengel F, Fernolend H, Schwaiger M, Nekolla S. Different CT protocols for attenuation correction in cardiac FDG imaging with PET/CT: a comparison with conventional PET [abstract]. *Eur J Nucl Med Mol Imaging.* 2004;31(suppl):S317.
48. Goerres GW, Ziegler SI, Burger C, Berthold T, Von Schulthess GK, Buck A. Artifacts at PET and PET/CT caused by metallic hip prosthetic material. *Radiology.* 2003;226:577–584.
49. Goerres GW, Kamel E, Heidelberg TN, Schwitter MR, Burger C, von Schulthess GK. PET-CT image co-registration in the thorax: influence of respiration. *Eur J Nucl Med Mol Imaging.* 2002;29:351–360.
50. Le Meunier L, Maarss-Moreno R, Carrasquillo J, et al. PET/CT imaging: effect of respiratory motion on ^{18}FDG myocardial uptake [abstract]. *J Nucl Med.* 2005;46(suppl):3P.
51. Makela T, Clarysse P, Sipila O, et al. A review of cardiac image registration methods. *IEEE Trans Med Imaging.* 2002;21:1011–1021.
52. Martinez Möller A, Martinez M, Ziegler SI, Navab N, Schwaiger M, Nekolla SG. Emission driven motion correction in PET/CT cardiac imaging [abstract]. *J Nucl Med.* 2005;46(suppl):163P.
53. Agatston AS, Janowitz WR, Kaplan G, Gasso J, Hildner F, Viamonte M Jr. Ultrafast computed tomography-detected coronary calcium reflects the angiographic extent of coronary arterial atherosclerosis. *Am J Cardiol.* 1994;74:1272–1274.
54. Mahnken AH, Koos R, Katoh M, et al. Sixteen-slice spiral CT versus MR imaging for the assessment of left ventricular function in acute myocardial infarction. *Eur Radiol.* 2005;15:714–720.
55. Schindler TH, Magosaki N, Jeserich M, et al. Fusion imaging: combined visualization of 3D reconstructed coronary artery tree and 3D myocardial scintigraphic image in coronary artery disease. *Int J Card Imaging.* 1999;15: 357–368.
56. Schindler TH, Nitzsche EU, Magosaki N, et al. Myocardial viability in patients with ischemic cardiomyopathy: evaluation by 3-D integration of myocardial scintigraphic data—and coronary angiographic data. *Mol Imaging Biol.* 2004; 6:160–171.
57. Faber TL, Santana CA, Garcia EV, et al. Three-dimensional fusion of coronary arteries with myocardial perfusion distributions: clinical validation. *J Nucl Med.* 2004;45:745–753.
58. Aladl UE, Hurwitz GA, Dey D, Levin D, Drangova M, Slomka PJ. Automated image registration of gated cardiac single-photon emission computed tomography and magnetic resonance imaging. *J Magn Reson Imaging.* 2004;19:283–290.
59. Namdar M, Hany TF, Koepfli P, et al. Integrated PET/CT for the assessment of coronary artery disease: a feasibility study. *J Nucl Med.* 2005;46:930–935.
60. Nekolla S, Souvatzoglou M, Hausleiter J, et al. Integration of function and morphology in cardiac PET/CT: a feasibility study in patients with chronic and ischemic heart disease [abstract. *J Nucl Cardiol.* 2005;12(suppl):S45.
61. Valentin J. *Annals of the ICRP: Publication 80.* Stockholm, Sweden: Pergamon; 1998.
62. Brix G, Lechel U, Glatting G, et al. Radiation exposure of patients undergoing whole-body dual-modality ^{18}F-FDG PET/CT examinations. *J Nucl Med.* 2005; 46:608–613.
63. Jakobs TF, Wintersperger BJ, Herzog P, et al. Ultra-low-dose coronary artery calcium screening using multislice CT with retrospective ECG gating. *Eur Radiol.* 2003;13:1923–1930.
64. Libby P. Current concepts of the pathogenesis of the acute coronary syndromes. *Circulation.* 2001;104:365–372.
65. Smith SC Jr, Dove JT, Jacobs AK, et al. ACC/AHA guidelines for percutaneous coronary intervention (revision of the 1993 PTCA guidelines): executive summary—a report of the American College of Cardiology/American Heart Association task force on practice guidelines (committee to revise the 1993 guidelines for percutaneous transluminal coronary angioplasty) endorsed by the Society for Cardiac Angiography and Interventions. *Circulation.* 2001;103: 3019–3041.
66. Choi HS, Choi BW, Choe KO, et al. Pitfalls, artifacts, and remedies in multidetector row CT coronary angiography. *Radiographics.* 2004;24:787–800.
67. Lau GT, Ridley LJ, Schieb MC, et al. Coronary artery stenoses: detection with calcium scoring, CT angiography, and both methods combined. *Radiology.* 2005;235:415–422.
68. Schmermund A, Erbel R. Non-invasive computed tomographic coronary angiography: the end of the beginning. *Eur Heart J.* 2005;26:1451–1453.
69. Achenbach S, Daniel WG. Computed tomography of the coronary arteries: more than meets the (angiographic) eye. *J Am Coll Cardiol.* 2005;46:155–157.
70. Chiurlia E, Menozzi M, Ratti C, Romagnoli R, Modena MG. Follow-up of coronary artery bypass graft patency by multislice computed tomography. *Am J Cardiol.* 2005;95:1094–1097.
71. Berman DS, Wong ND, Gransar H, et al. Relationship between stress-induced

myocardial ischemia and atherosclerosis measured by coronary calcium tomography. *J Am Coll Cardiol.* 2004;44:923–930.
72. Bergmann SR, Fox KA, Rand AL, et al. Quantification of regional myocardial blood flow in vivo with $H_2{}^{15}O$. *Circulation.* 1984;70:724–733.
73. Law I, Iida H, Holm S, et al. Quantitation of regional cerebral blood flow corrected for partial volume effect using O-15 water and PET: II. Normal values and gray matter blood flow response to visual activation. *J Cereb Blood Flow Metab.* 2000;20:1252–1263.
74. Goldstein RA, Mullani NA, Marani SK, Fisher DJ, Gould KL, O'Brien HA Jr. Myocardial perfusion with rubidium-82. II. Effects of metabolic and pharmacologic interventions. *J Nucl Med.* 1983;24:907–915.
75. Parkash R, deKemp RA, Ruddy TD, et al. Potential utility of rubidium 82 PET quantification in patients with 3-vessel coronary artery disease. *J Nucl Cardiol.* 2004;11:440–449.
76. Beanlands RS, Muzik O, Melon P, et al. Noninvasive quantification of regional myocardial flow reserve in patients with coronary atherosclerosis using nitrogen-13 ammonia positron emission tomography: determination of extent of altered vascular reactivity. *J Am Coll Cardiol.* 1995;26:1465–1475.
77. Muzik O, Paridon SM, Singh TP, Morrow WR, Dayanikli F, Di Carli MF. Quantification of myocardial blood flow and flow reserve in children with a history of Kawasaki disease and normal coronary arteries using positron emission tomography. *J Am Coll Cardiol.* 1996;28:757–762.
78. Kuhle WG, Porenta G, Huang SC, et al. Quantification of regional myocardial blood flow using ^{13}N-ammonia and reoriented dynamic positron emission tomographic imaging. *Circulation.* 1992;86:1004–1017.
79. Yoshinaga K, Katoh C, Noriyasu K, et al. Reduction of coronary flow reserve in areas with and without ischemia on stress perfusion imaging in patients with coronary artery disease: a study using oxygen 15-labeled water PET. *J Nucl Cardiol.* 2003;10:275–283.
80. Conaway D, Bateman T, Moutray K, et al. Impact of myocardial perfusion PET following non-diagnostic SPECT: follow-up procedures and patient outcomes [abstract]. *J Nucl Med.* 2005;46(suppl):58P.
81. Lloyd-Jones DM, O'Donnell CJ, D'Agostino RB, Massaro J, Silbershatz H, Wilson PW. Applicability of cholesterol-lowering primary prevention trials to a general population: the Framingham heart study. *Arch Intern Med.* 2001;161:949–954.
82. Cooper JA, Miller GJ, Humphries SE. A comparison of the PROCAM and Framingham point-scoring systems for estimation of individual risk of coronary heart disease in the Second Northwick Park Heart Study. *Atherosclerosis.* 2005;181:93–100.
83. Grundy SM. The changing face of cardiovascular risk. *J Am Coll Cardiol.* 2005;46:173–175.
84. Pletcher MJ, Tice JA, Pignone M, Browner WS. Using the coronary artery calcium score to predict coronary heart disease events: a systematic review and meta-analysis. *Arch Intern Med.* 2004;164:1285–1292.
85. Greenland P, LaBree L, Azen SP, Doherty TM, Detrano RC. Coronary artery calcium score combined with Framingham score for risk prediction in asymptomatic individuals. *JAMA.* 2004;291:1831–1832.
86. Shaw LJ, Raggi P, Schisterman E, Berman DS, Callister TQ. Prognostic value of cardiac risk factors and coronary artery calcium screening for all-cause mortality. *Radiology.* 2003;228:826–833.
87. Raggi P, Shaw LJ, Berman DS, Callister TQ. Prognostic value of coronary artery calcium screening in subjects with and without diabetes. *J Am Coll Cardiol.* 2004;43:1663–1669.
88. Anand DV, Lim E, Raval U, Lipkin D, Lahiri A. Prevalence of silent myocardial ischemia in asymptomatic individuals with subclinical atherosclerosis detected by electron beam tomography. *J Nucl Cardiol.* 2004;11:450–457.
89. Dayanikli F, Grambow D, Muzik O, Mosca L, Rubenfire M, Schwaiger M. Early detection of abnormal coronary flow reserve in asymptomatic men at high risk for coronary artery disease using positron emission tomography. *Circulation.* 1994;90:808–817.
90. Laaksonen R, Janatuinen T, Vesalainen R, et al. High oxidized LDL and elevated plasma homocysteine contribute to the early reduction of myocardial flow reserve in healthy adults. *Eur J Clin Invest.* 2002;32:795–802.
91. Yokoyama I, Murakami T, Ohtake T, et al. Reduced coronary flow reserve in familial hypercholesterolemia. *J Nucl Med.* 1996;37:1937–1942.
92. Mauriello A, Sangiorgi G, Fratoni S, et al. Diffuse and active inflammation occurs in both vulnerable and stable plaques of the entire coronary tree: a histopathologic study of patients dying of acute myocardial infarction. *J Am Coll Cardiol.* 2005;45:1585–1593.
93. Uren NG, Crake T, Lefroy DC, de Silva R, Davies GJ, Maseri A. Reduced coronary vasodilator function in infarcted and normal myocardium after myocardial infarction. *N Engl J Med.* 1994;331:222–227.
94. Schachinger V, Zeiher AM. Prognostic implications of endothelial dysfunction: does it mean anything? *Coron Artery Dis.* 2001;12:435–443.
95. Schindler TH, Hornig B, Buser PT, et al. Prognostic value of abnormal vasoreactivity of epicardial coronary arteries to sympathetic stimulation in patients with normal coronary angiograms. *Arterioscler Thromb Vasc Biol.* 2003;23:495–501.
96. Halcox JP, Schenke WH, Zalos G, et al. Prognostic value of coronary vascular endothelial dysfunction. *Circulation.* 2002;106:653–658.
97. Guethlin M, Kasel AM, Coppenrath K, Ziegler S, Delius W, Schwaiger M. Delayed response of myocardial flow reserve to lipid-lowering therapy with fluvastatin. *Circulation.* 1999;99:475–481.
98. Huggins GS, Pasternak RC, Alpert NM, Fischman AJ, Gewirtz H. Effects of short-term treatment of hyperlipidemia on coronary vasodilator function and myocardial perfusion in regions having substantial impairment of baseline dilator reverse. *Circulation.* 1998;98:1291–1296.
99. Yokoyama I, Yonekura K, Inoue Y, Ohtomo K, Nagai R. Long-term effect of simvastatin on the improvement of impaired myocardial flow reserve in patients with familial hypercholesterolemia without gender variance. *J Nucl Cardiol.* 2001;8:445–451.
100. Janatuinen T, Laaksonen R, Vesalainen R, et al. Effect of lipid-lowering therapy with pravastatin on myocardial blood flow in young mildly hypercholesterolemic adults. *J Cardiovasc Pharmacol.* 2001;38:561–568.
101. Maniscalco BS, Taylor KA. Calcification in coronary artery disease can be reversed by EDTA-tetracycline long-term chemotherapy. *Pathophysiology.* 2004;11:95–101.
102. Petronio AS, Amoroso G, Limbruno U, et al. Simvastatin does not inhibit intimal hyperplasia and restenosis but promotes plaque regression in normocholesterolemic patients undergoing coronary stenting: a randomized study with intravascular ultrasound. *Am Heart J.* 2005;149:520–526.
103. Achenbach S, Moselewski F, Ropers D, et al. Detection of calcified and noncalcified coronary atherosclerotic plaque by contrast-enhanced, submillimeter multidetector spiral computed tomography: a segment-based comparison with intravascular ultrasound. *Circulation.* 2004;109:14–17.
104. Rutt CD, Coleman KJ. Examining the relationships among built environment, physical activity, and body mass index in El Paso, TX. *Prev Med.* 2005;40:831–841.
105. Patel NA, Stamper DL, Brezinski ME. Review of the ability of optical coherence tomography to characterize plaque, including a comparison with intravascular ultrasound. *Cardiovasc Intervent Radiol.* 2005;28:1–9.
106. Becker CR, Nikolaou K, Muders M, et al. Ex vivo coronary atherosclerotic plaque characterization with multi-detector-row CT. *Eur Radiol.* 2003;13:2094–2098.
107. Rudd JH, Warburton EA, Fryer TD, et al. Imaging atherosclerotic plaque inflammation with [^{18}F]-fluorodeoxyglucose positron emission tomography. *Circulation.* 2002;105:2708–2711.
108. Schafers M, Dutka D, Rhodes CG, et al. Myocardial presynaptic and postsynaptic autonomic dysfunction in hypertrophic cardiomyopathy. *Circ Res.* 1998;82:57–62.
109. Strauss HW, Grewal RK, Pandit-Taskar N. Molecular imaging in nuclear cardiology. *Semin Nucl Med.* 2004;34:47–55.
110. Kolodgie FD, Petrov A, Virmani R, et al. Targeting of apoptotic macrophages and experimental atheroma with radiolabeled annexin V: a technique with potential for noninvasive imaging of vulnerable plaque. *Circulation.* 2003;108:3134–3139.
111. Blankenberg FG, Strauss HW. Will imaging of apoptosis play a role in clinical care? A tale of mice and men. *Apoptosis.* 2001;6:117–123.
112. Narula J, Strauss HW. Imaging of unstable atherosclerotic lesions. *Eur J Nucl Med Mol Imaging.* 2005;32:1–5.
113. Gawaz M, Konrad I, Hauser AI, et al. Non-invasive imaging of glycoprotein VI binding to injured arterial lesions. *Thromb Haemost.* 2005;93:910–913.
114. Botnar RM, Perez AS, Witte S, et al. In vivo molecular imaging of acute and subacute thrombosis using a fibrin-binding magnetic resonance imaging contrast agent. *Circulation.* 2004;109:2023–2029.
115. Piccini JP, Klein L, Gheorghiade M, Bonow RO. New insights into diastolic heart failure: role of diabetes mellitus. *Am J Med.* 2004;116(suppl 5A):64S–75S.
116. Di Carli MF, Asgarzadie F, Schelbert HR, et al. Quantitative relation between myocardial viability and improvement in heart failure symptoms after revascularization in patients with ischemic cardiomyopathy. *Circulation.* 1995;92:3436–3444.
117. Allman KC, Shaw LJ, Hachamovitch R, Udelson JE. Myocardial viability testing and impact of revascularization on prognosis in patients with coronary

artery disease and left ventricular dysfunction: a meta-analysis. *J Am Coll Cardiol.* 2002;39:1151–1158.
118. Di Carli MF, Maddahi J, Rokhsar S, et al. Long-term survival of patients with coronary artery disease and left ventricular dysfunction: implications for the role of myocardial viability assessment in management decisions. *J Thorac Cardiovasc Surg.* 1998;116:997–1004.
119. Eitzman D, al-Aouar Z, Kanter HL, et al. Clinical outcome of patients with advanced coronary artery disease after viability studies with positron emission tomography. *J Am Coll Cardiol.* 1992;20:559–565.
120. Haas F, Haehnel CJ, Picker W, et al. Preoperative positron emission tomographic viability assessment and perioperative and postoperative risk in patients with advanced ischemic heart disease. *J Am Coll Cardiol.* 1997;30:1693–1700.
121. Hundt W, Siebert K, Wintersperger BJ, et al. Assessment of global left ventricular function: comparison of cardiac multidetector-row computed tomography with angiocardiography. *J Comput Assist Tomogr.* 2005;29:373–381.
122. Wagner B, Reder S, Anton M, et al. Hybrid PET/CT for functional/biological characterization of myocardial molecular interventions: a multi-tracer study in a pig model of adenoviral VEGF gene transfer [abstract]. *J Nucl Med.* 2005; 46(suppl):1P.
123. Hunold P, Vogt FM, Schmermund A, et al. Radiation exposure during cardiac CT: effective doses at multi-detector row CT and electron-beam CT. *Radiology.* 2003;226:145–152.
124. Wu TH, Huang YH, Lee JJ, et al. Radiation exposure during transmission measurements: comparison between CT- and germanium-based techniques with a current PET scanner. *Eur J Nucl Med Mol Imaging.* 2004;31:38–43.
125. Schelbert HR, Wisenberg G, Phelps ME, et al. Noninvasive assessment of coronary stenoses by myocardial imaging during pharmacologic coronary vasodilation. VI. Detection of coronary artery disease in human beings with intravenous N-13 ammonia and positron computed tomography. *Am J Cardiol.* 1982;49:1197–1207.
126. Tamaki N, Yonekura Y, Senda M, et al. Value and limitation of stress thallium-201 single photon emission computed tomography: comparison with nitrogen-13 ammonia positron tomography. *J Nucl Med.* 1988;29:1181–1188.
127. Muzik O, Duvernoy C, Beanlands RS, et al. Assessment of diagnostic performance of quantitative flow measurements in normal subjects and patients with angiographically documented coronary artery disease by means of nitrogen-13 ammonia and positron emission tomography. *J Am Coll Cardiol.* 1998;31:534–540.
128. Go RT, Marwick TH, MacIntyre WJ, et al. A prospective comparison of rubidium-82 PET and thallium-201 SPECT myocardial perfusion imaging utilizing a single dipyridamole stress in the diagnosis of coronary artery disease. *J Nucl Med.* 1990;31:1899–1905.
129. Stewart RE, Schwaiger M, Molina E, et al. Comparison of rubidium-82 positron emission tomography and thallium-201 SPECT imaging for detection of coronary artery disease. *Am J Cardiol.* 1991;67:1303–1310.
130. Grover-McKay M, Ratib O, Schwaiger M, et al. Detection of coronary artery disease with positron emission tomography and rubidium 82. *Am Heart J.* 1992;123:646–652.
131. Marwick TH, Nemec JJ, Stewart WJ, Salcedo EE. Diagnosis of coronary artery disease using exercise echocardiography and positron emission tomography: comparison and analysis of discrepant results. *J Am Soc Echocardiogr.* 1992;5:231–238.